

## HOLE SPIN SURFACES IN WURTZITE SEMICONDUCTORS

A. Dargys

*Semiconductor Physics Institute, A. Goštauto 11, LT-01108 Vilnius, Lithuania*

E-mail: dargys@pfi.lt

Received 15 October 2004

Spin properties of holes in the wurtzite semiconductors, when the hole with a given wave vector ballistically propagates in either heavy-, light-mass or crystal-field split-off band, are considered. Analytical solutions for an averaged hole spin are found for two important cases, when the hole wave vector is parallel and perpendicular to the hexagonal axis. Shapes of the spin surfaces are presented for these cases. It is shown that the surfaces, in general, are spheroids. However, depending on the wave vector magnitude and valence band parameters, the surfaces may also be spheres or line-shaped. The properties of the spin surfaces are illustrated for parameters of the wurtzite GaN, where the crystal field dominates in the splitting of the valence band.

**Keywords:** wurtzites, spintronics, valence band, spin, GaN

**PACS:** 71.70.Ms, 72.20.Jv, 73.40.Gk, 78.55.-m, 79.90.+b

### 1. Introduction

Electron and hole spin properties in wide-bandgap semiconductors are of a special interest due to their potential application in spin-transport electronics (spintronics) in which the spin of free carriers is used to provide new functionality in the micro- or nanoelectronic devices [1]. GaN, GaP, and ZnO semiconductors doped with Mn impurity can be used to obtain electrically controlled magnetic sensors, actuators, and spin injectors in all-semiconductor devices [2]. The high spin injection efficiency from ferromagnetic semiconductors into undoped semiconductor allows one to fabricate spin-polarized light emitters for optical encoding, advanced optical switches, and modulators. A useful property of the wide-bandgap nitride semiconductors doped with magnetic impurities, such as GaN, AlN or InN, is their high Curie temperature. In GaN, for example, the Curie temperature exceeds 400 K [2, 3].

The spin properties of the valence band holes in elementary and  $A_3B_5$  cubic semiconductors were considered recently in [4–6], where it was shown that the form of a spin surface of heavy- and light-mass band holes strongly deviates from the sphere, and that this deviation can explain large anisotropy of spin injection efficiency observed in cubic semiconductors in [7]. The concept of the spin surface appears especially useful in explaining hole spin properties in ultrafast hole spin

switching dynamics by high electric fields [8–10]. In the general case, the spin trajectory in the spin space may be very complicated when the hole undergoes an interband transition. The knowledge of the shape of the spin surface allows one to identify the initial and final states of the hole wave function on the spin trajectory where spin evolution takes place.

In this paper we shall be interested in spin properties of holes injected into a pure wurtzite semiconductor, when the concentration of the injected holes is small. The latter assumption allows one to treat the problem within a single particle frame. As known, the wide-bandgap nitride materials are grown in both zincblende (cubic) and wurtzite (hexagonal) polytypes. However, in the device application the wurtzite structure is the most interesting. In this paper the spin properties of heavy, light, and crystal-field holes in wurtzite-type semiconductors are presented only. For a general direction of the wave vector the problem can be solved only by numerical methods. Therefore, in this paper we shall limit ourselves to two practically important situations that can be treated analytically, namely, when the wave vector of a ballistic hole is either parallel or perpendicular to crystal hexagonal axis. In the next section the properties of the wurtzite-type Hamiltonian in the standard basis are discussed first and then in the subsequent section they are used for constructing a unitary transformation matrix that connects basis wave functions in standard and energy represen-

tations. The knowledge of the transformation matrix will allow us to find spin surfaces for all three energy bands.

## 2. Wurtzite Hamiltonian and spin matrices

In wide-gap wurtzites the structure of the uppermost, situated near the Brillouin zone centre, valence band is determined by two competing mechanisms, the crystal-field interaction and the spin–orbit interaction. In the lowest approximation of the envelope-function formalism [11], when valence band splitting is omitted, in the vicinity of the  $\Gamma_{15}$  symmetry point one has three (doubly degenerate) valence bands (see Fig. 1). In the zinc-blende-type cubic semiconductors the crystal-field component is absent and the valence band splitting at the wave vector  $\mathbf{k} \approx 0$  is determined by spin–orbit interaction only, as the left-hand side of Fig. 1 shows. In the wurtzite semiconductors, the hexagonal component of the crystal field is relatively large (right-hand side of Fig. 1). As a result of the action of the crystal field (cr) and weaker spin–orbit (so) mechanisms, the heavy- and light-mass degeneracy is lifted off. Thus, in the wurtzite semiconductor all three bands – heavy-hole (HH), light-hole (LH), and split-off hole (SH) – are separated by respective energy gaps.

Inclusion of a finite value of the hole wave vector usually is done by the  $\mathbf{k}\cdot\mathbf{p}$  theory [12] or invariant method [11]. Using the spherical harmonic representation given by the basis functions  $Y_{pm}$ ,

$$|Y\rangle = \{|Y_{11}\uparrow\rangle, |Y_{11}\downarrow\rangle, |Y_{10}\uparrow\rangle, |Y_{10}\downarrow\rangle, |Y_{1-1}\uparrow\rangle, |Y_{1-1}\downarrow\rangle\}^T, \quad (1)$$

where up and down arrows indicate the hole spin state, one obtains the following effective-mass Hamiltonian matrix for a wurtzite-type valence band [11, 13–15]:

$$\hat{H} = \begin{bmatrix} F & 0 & -H^* & 0 & K^* & 0 \\ 0 & G & \Delta & -H^* & 0 & K^* \\ -H & \Delta & \lambda & 0 & \Pi^* & 0 \\ 0 & -H & 0 & \lambda & \Delta & \Pi^* \\ K & 0 & \Pi & \Delta & G & 0 \\ 0 & K & 0 & \Pi & 0 & F \end{bmatrix}. \quad (2)$$

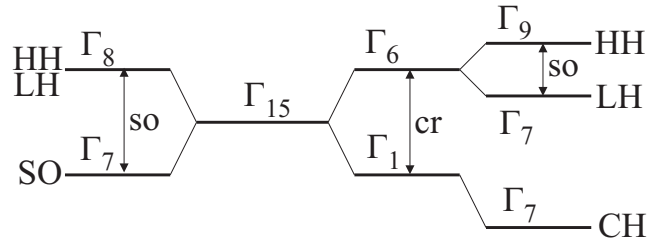


Fig. 1. Valence band structure in zinc-blende (cubic) and wurtzite (hexagonal) nitrides at  $\mathbf{k} = 0$ . In the crystals of the cubic symmetry the bands  $\Gamma_8$  (heavy-hole HH and light-hole LH) and  $\Gamma_7$  (spin-orbit split-off hole SO) are separated because of spin–orbit (so) interaction. In the wurtzite symmetry crystals the bands of symmetry  $\Gamma_6$  and  $\Gamma_1$  are due to hexagonal component of the crystal (cr) field. An additional splitting of  $\Gamma_6$  to  $\Gamma_9$  and  $\Gamma_7$  comes from the spin–orbit interaction. CH is the crystal-field split-off hole band.

The components of the matrix in atomic units ( $e = \hbar = m_0 = 1$ ) are given by

$$\begin{aligned} F &= \Delta_1 + \Delta_2 + \lambda + \theta, \\ G &= \Delta_1 - \Delta_2 + \lambda + \theta, \\ \lambda &= \frac{A_1 k_z^2 + A_2 (k_x^2 + k_y^2)}{2}, \\ \theta &= \frac{A_3 k_z^2 + A_4 (k_x^2 + k_y^2)}{2}, \\ K &= \frac{A_5 (k_x + ik_y)^2}{2}, \\ H &= \left( \frac{iA_6 k_z}{2} - A_7 \right) (k_x + ik_y), \\ \Pi &= \left( \frac{iA_6 k_z}{2} + A_7 \right) (k_x + ik_y), \\ \Delta &= \Delta_3 \sqrt{2}. \end{aligned} \quad (3)$$

In the Hamiltonian (2) the  $k_z$  axis was chosen to be parallel to  $c$  axis, i. e. (0001) crystallographic axis that has a sixfold symmetry in the wurtzite semiconductors. If  $A_7 = 0$ , one can show that all bands are doubly (spin) degenerate. The eigenvalues of Eqs. (2) and (3) give the dependence of band energies on the wave vector  $\mathbf{k}$ . Figures 2 and 3 show HH, LH, and CH bands, when the wave vector is either parallel or perpendicular to  $c$  axis. The parameters of GaN were used in the numerical calculations (see Table 1). A characteristic feature to be noted in Fig. 2, when  $\mathbf{k}$  is perpendicular to  $c$  axis, is the intersection of LH and CH bands at  $\mathbf{k}$  that corresponds to thermal hole energies. Very strong

Table 1. The effective-mass parameters for the valence band of wurtzite GaN:  $\Delta_i$ 's are in units of meV,  $A_i$ 's are in atomic units (or in units of  $\hbar^2/m_0$ ) except for  $A_7$  which is in units of eV/Å [14].

Parameter	Value
$\Delta_1$	21.2
$\Delta_2$	3.61
$\Delta_3$	3.61
$A_1$	-7.21
$A_2$	-0.440
$A_3$	6.66
$A_4$	-3.46
$A_5$	-3.40
$A_6$	-4.9
$A_7$	0.0937

nonparabolicity of the bands is observed at these energies.

In [14] it was shown that the Hamiltonian (2) can be block-diagonalized, even when  $A_7 \neq 0$ , if new basis functions (in the following referred to as  $v$ -basis) are chosen:

$$\begin{aligned}
 |v_1\rangle &= \alpha^* |Y_{11} \uparrow\rangle - \alpha |Y_{1-1} \downarrow\rangle, \\
 |v_2\rangle &= \beta |Y_{1-1} \uparrow\rangle - \beta^* |Y_{11} \downarrow\rangle, \\
 |v_3\rangle &= -\beta^* |Y_{10} \uparrow\rangle + \beta |Y_{10} \downarrow\rangle, \\
 |v_4\rangle &= \alpha^* |Y_{11} \uparrow\rangle + \alpha |Y_{1-1} \downarrow\rangle, \\
 |v_5\rangle &= \beta |Y_{1-1} \uparrow\rangle + \beta^* |Y_{11} \downarrow\rangle, \\
 |v_6\rangle &= -\beta^* |Y_{10} \uparrow\rangle + \beta |Y_{10} \downarrow\rangle,
 \end{aligned} \tag{4}$$

where  $\alpha = \exp(-i3\phi/2)\sqrt{2}$ ,  $\beta = \exp(-i\phi/2)\sqrt{2}$ . The angle  $\phi$  is defined as  $\phi = \tan^{-1}(k_x/k_y)$ , where  $k_x$  and  $k_y$  are hole wave vector components perpendicular to  $c$  axis. It should be noted that some of the exponential terms in Eq. (4) have opposite sign to that in [14]. It is convenient to perform the transformation of the  $6 \times 6$  Hamiltonian (2) to basis (4) using the following unitary matrix:

$$\hat{U} = \begin{bmatrix} \alpha^* & 0 & 0 & 0 & 0 & \alpha \\ 0 & -\beta^* & 0 & 0 & \beta & 0 \\ 0 & 0 & -\beta^* & \beta & 0 & 0 \\ \alpha^* & 0 & 0 & 0 & 0 & \alpha \\ 0 & \beta^* & 0 & 0 & \beta & 0 \\ 0 & 0 & \beta^* & \beta & 0 & 0 \end{bmatrix}. \tag{5}$$

Then, in the block-diagonalized Hamiltonian  $\hat{H}_{U,L} = \hat{U}\hat{H}\hat{U}^\dagger$ , the upper  $3 \times 3$  block  $\hat{H}_U$  assumes the following form:

$$\hat{H}_U = \frac{1}{2} \times \begin{bmatrix} \varepsilon + 2(\Delta_1 + \Delta_2) & A_5 k_t^2 & -(2A_7 + iA_6 k_z) k_t \\ A_5 k_t^2 & \varepsilon + 2(\Delta_1 - \Delta_2) & -(2A_7 + iA_6 k_z) k_t + \sqrt{2}\Delta_3 \\ -(2A_7 - iA_6 k_z) k_t & -(2A_7 - iA_6 k_z) k_t & -A_2 k_t^2 + A_1 k_z^2 + \sqrt{2}\Delta_3 \end{bmatrix}, \tag{6}$$

where  $\varepsilon = (A_2 + A_4)k_t^2 + (A_1 + A_3)k_z^2$  and  $k_t^2 = k_x^2 + k_y^2$ . The lower block  $\hat{H}_L$  can be obtained from the upper block  $\hat{H}_U$ , if the sign of  $k_t$  is changed to the opposite. At  $\mathbf{k} = 0$ , from  $\hat{H}_U$  and  $\hat{H}_L$  one finds that the hole energies at the band edges CH, LH, and HH shown in Fig. 1, respectively, can be expressed through  $\Delta$ 's only:

$$\begin{aligned}
 E_{c0} &= \frac{1}{2} \left[ (\Delta_1 - \Delta_2) - \sqrt{8\Delta_3 + (\Delta_1 - \Delta_2)^2} \right], \\
 E_{l0} &= \frac{1}{2} \left[ (\Delta_1 - \Delta_2) + \sqrt{8\Delta_3 + (\Delta_1 - \Delta_2)^2} \right], \\
 E_{h0} &= \Delta_1 + \Delta_2.
 \end{aligned} \tag{7}$$

As Table 1 shows, in GaN one has  $\Delta_1 \gg \Delta_2, \Delta_3$ , and as a result,  $E_{h0} \approx E_{l0} \sim \Delta_1$ . Thus, in GaN heavy- and light-hole bands in the vicinity of  $\mathbf{k} = 0$  point are nearly degenerate, while the crystal-field band is split off by the energy  $\Delta_1$ . If  $A_7 = 0$ , then  $\Pi = H$ , and all linear- $\mathbf{k}$  terms vanish. As mentioned, in this case the bands become doubly degenerate by the spin quantum number. In the next section the obtained expressions for  $\hat{H}_U$  and  $\hat{H}_L$  will be used to find the analytical approximations to the unitary matrix that connects  $v$  basis and energy basis where the Hamiltonian is diagonal, with the diagonal elements representing the dispersions of HH, LH, and CH bands.

To calculate hole spin surfaces for different bands and various wave vectors, we need  $6 \times 6$  spin matrices  $S_i$  in one of the mentioned representation basis. The simplest expression for  $S_i$  is obtained in the basis given by Eq. (1), since the components of the hole spin in this basis can be expressed through pure states. In basis (1) the spin matrices can be calculated as a direct product of  $3 \times 3$  unit matrix  $I_{3 \times 3}$  and Pauli matrices  $\sigma_i$ :

$$S_i = I_{3 \times 3} \otimes \sigma_i / 2. \tag{8}$$

### 3. Transformation matrices

The next goal is to find a unitary transformation matrix that diagonalizes  $3 \times 3$  Hamiltonians  $\hat{H}_U$  and  $\hat{H}_L$ . Such a unitary matrix, in principle, can be constructed from the eigenvectors of  $\hat{H}_U$  and  $\hat{H}_L$  using the algebra manipulation system, for example, such as *Mathematica*. However, the obtained eigenvectors have been found to be very complicated to have any practical usage. By this reason below two special cases – when the wave vector is either perpendicular or parallel to the hexagonal axis – will be considered. Under some simplifying additional assumptions, then, it appears possible to find analytically tractable expressions.

#### 3.1. $k \perp c$ case

In this case  $k_z = 0$ . However, even under this simplifying condition the eigenvalues and eigenvectors of the resulting  $3 \times 3$  matrices are still expressed through cubic roots and are rather complicated. The cubic roots remain if one assumes that the bands are doubly degenerate, i. e. that  $A_7 = 0$ . If, in addition, the coefficient  $\Delta_3$  is equated to zero, the eigenvalues and eigenvectors become relatively simple. Thus, under the assumptions  $k_z = 0$ ,  $A_7 = 0$ , and  $\Delta_3 = 0$ , the bands that result from  $\hat{H}_U$  and  $\hat{H}_L$  become doubly degenerate and have the following dispersion laws in the directions perpendicular to the  $c$  axis:

$$\begin{aligned} E_{c\perp} &= \frac{A_2 k_t^2}{2}, \\ E_{l\perp} &= \frac{(A_2 + A_4)k_t^2 + 2\Delta_1 - s}{2}, \\ E_{h\perp} &= \frac{(A_2 + A_4)k_t^2 + 2\Delta_1 + s}{2}, \end{aligned} \quad (9)$$

where  $s = \sqrt{A_3^2 k_t^4 + 4\Delta_2^2}$  and the subscripts  $c$ ,  $l$ , and  $h$  indicate the crystal-field split-off, light-mass and heavy-mass bands, respectively. Under these approximations, the band-edge energies at  $k_t = 0$  are  $E_{c0} = 0$ ,  $E_{l0} = \Delta_1 - \Delta_2$ , and  $E_{h0} = \Delta_1 + \Delta_2$  which are to be compared with the exact expression (7). Normally  $\Delta_1 \gg \Delta_2$  (see, for example, Table 1), and the band edge of the crystal-field split-off band appears to be far below the heavy- and light-hole band edges. The squares, diamonds, and stars in Fig. 2 show the dispersion curves given by Eqs. (9). It is seen that for GaN, except the region where LH and CH bands are crossing, they are very close to the true dispersion curves (lines) calculated numerically with the initial Hamiltonian (2). Thus, in this approximation the parameter  $\Delta_1$

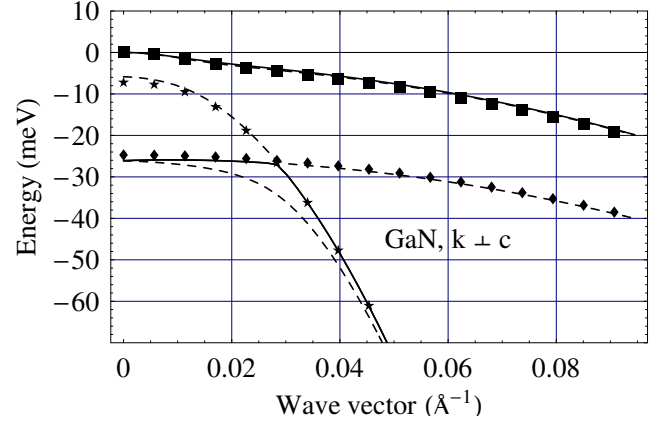


Fig. 2. Valence band structure of the wurtzite GaN when the hole wave vector is perpendicular to  $c$  axis. The points were calculated with the approximate formulas (9). All energies are shifted down, so that at  $k_t = 0$  the band edge of the HH band is at zero.

describes the crystal splitting and  $\Delta_2$  describes heavy- and light-mass band spin-orbit splitting at the centre of the Brillouin zone. The intersection of the light-mass LH and crystal-split CH branches occurs at the wave vector

$$k_t = \sqrt{\frac{-2A_4\Delta_1 - 2\sqrt{A_4^2\Delta_2^2 + A_5^2(\Delta_1^2 - \Delta_2^2)}}{A_4^2 - A_5^2}}. \quad (10)$$

Under the mentioned approximations, using the eigenvectors of  $3 \times 3$  Hamiltonians, now it is easy to find the unitary transformation matrix  $T_\perp$  that transforms the initial Hamiltonian (2) to its diagonal form:

$$\begin{aligned} \hat{H}_{\text{diag}} &= T_\perp \hat{H} T_\perp^\dagger \\ &= \{E_{c\perp}, E_{l\perp}, E_{h\perp}, E_{c\perp}, E_{l\perp}, E_{h\perp}\}. \end{aligned} \quad (11)$$

The energies in the last expression show the order of the valence bands in the diagonal Hamiltonian  $\hat{H}_{\text{diag}}$ . The required transformation matrix is

$$T_\perp = \begin{bmatrix} 0 & 0 & -\frac{e^{i\phi/2}}{\sqrt{2}} & \frac{e^{-i\phi/2}}{\sqrt{2}} & 0 & 0 \\ -t(-)e^{3i\phi/2} & -\frac{e^{i\phi/2}}{2r(+)} & 0 & 0 & \frac{e^{-i\phi/2}}{2r(+)} & t(-)e^{-3i\phi/2} \\ t(+ )e^{3i\phi/2} & -\frac{e^{i\phi/2}}{2r(-)} & 0 & 0 & \frac{e^{-i\phi/2}}{2r(-)} & -t(+ )e^{-3i\phi/2} \\ 0 & 0 & \frac{e^{i\phi/2}}{\sqrt{2}} & \frac{e^{-i\phi/2}}{\sqrt{2}} & 0 & 0 \\ -t(-)e^{3i\phi/2} & \frac{e^{i\phi/2}}{2r(+)} & 0 & 0 & \frac{e^{-i\phi/2}}{2r(+)} & -t(-)e^{-3i\phi/2} \\ t(+ )e^{3i\phi/2} & \frac{e^{i\phi/2}}{2r(-)} & 0 & 0 & \frac{e^{-i\phi/2}}{2r(-)} & t(+ )e^{-3i\phi/2} \end{bmatrix}, \quad (12)$$

where  $r^{(\pm)} = \sqrt{s/(s \pm 2\Delta_2)}$  and  $t^{(\pm)} = (s \pm 2\Delta_2)/(2A_5k_t^2r^{(\mp)})$ . Since  $s$  and  $\phi$  depend on the transverse wave vector, the transformation matrix (12) depends on  $k_x$  and  $k_y$ , too. This property implies that the shape of spin surfaces in the wurtzite-type semiconductors will depend on the magnitude of the hole wave vector. This property was also found in zinc-blende semiconductors, too [5, 6].

### 3.2. $\mathbf{k} \parallel c$ case

Now  $k_t = 0$ , and the hole is moving along  $c$  axis. No approximations are needed in this case. Both Hamiltonians,  $\hat{H}_U$  and  $\hat{H}_L$ , give the same dispersion laws:

$$\begin{aligned} E_{h\parallel} &= \frac{1}{2}(A_1 + A_3)k_z^2 + \Delta_1 + \Delta_2, \\ E_{c\parallel} &= \frac{1}{4}[2A_1k_z^2 + u - w], \\ E_{l\parallel} &= \frac{1}{4}[2A_1k_z^2 + u + w], \end{aligned} \quad (13)$$

where

$$u = A_3k_z^2 + 2\Delta_1 - 2\Delta_2, \quad (14)$$

$$w = \sqrt{u^2 + 32\Delta_3^2}. \quad (15)$$

The dispersions (13) are exact and, therefore, they coincide with those calculated numerically using the initial Hamiltonian (2) and shown in Fig. 3 by lines. When  $\mathbf{k} \parallel c$  the bands do not cross, although as seen from Eqs. (13)–(15), they are nonparabolic. The unitary transformation matrix  $T_{\parallel}$  that diagonalizes the initial Hamiltonian (2),  $\hat{H}_{\text{diag}} = T_{\parallel}\hat{H}T_{\parallel}^{\dagger} = \{E_{c\parallel}, E_{l\parallel}, E_{h\parallel}, E_{c\parallel}, E_{l\parallel}, E_{h\parallel}\}$ , in this case is

$$T_{\parallel} = \begin{bmatrix} 0 & -\frac{u-w}{2v^{(-)}} & -\frac{4\Delta_3}{s^{(-)}} & \frac{4\Delta_3}{s^{(-)}} & \frac{u-w}{2v^{(-)}} & 0 \\ 0 & -\frac{u+w}{2v^{(+)}} & -\frac{4\Delta_3}{s^{(+)}} & \frac{4\Delta_3}{s^{(+)}} & \frac{u+w}{2v^{(+)}} & 0 \\ \frac{1}{\sqrt{2}} & 0 & 0 & 0 & 0 & -\frac{1}{\sqrt{2}} \\ 0 & \frac{u-w}{2v^{(-)}} & \frac{4\Delta_3}{s^{(-)}} & \frac{4\Delta_3}{s^{(-)}} & \frac{u-w}{2v^{(-)}} & 0 \\ 0 & \frac{u+w}{2v^{(+)}} & \frac{4\Delta_3}{s^{(+)}} & \frac{4\Delta_3}{s^{(+)}} & \frac{u+w}{2v^{(+)}} & 0 \\ \frac{1}{\sqrt{2}} & 0 & 0 & 0 & 0 & \frac{1}{\sqrt{2}} \end{bmatrix}, \quad (16)$$

where

$$v^{(\pm)} = \sqrt{u(u \pm w) + 32\Delta_3^2}, \quad (17)$$

$$s^{(\pm)} = \sqrt{(u \pm w)^2 + 32\Delta_3^2}. \quad (18)$$

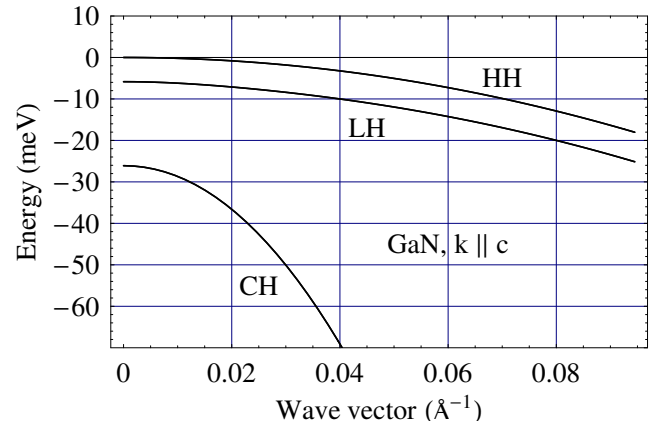


Fig. 3. Valence band structure of the wurtzite GaN when the hole wave vector is parallel to  $c$  axis.

Since the dispersion laws (13) are exact the transformation matrix (16), which is intimately related with (13) through the eigenvectors used in constructing the transformation matrix, is exact, too.

## 4. Spin surfaces

The spin surface describes all possible locations of the end of the average spin  $\mathbf{S}$ , or total angular momentum  $\mathbf{J}$ , of the carrier when the state vector that represents a given band  $n$  and the wave vector  $\mathbf{k}$  is parametrized [5, 6]. For a free electron the spin surface is a sphere of radius  $1/2$  described by components  $(\langle S_x \rangle, \langle S_y \rangle, \langle S_z \rangle)$  in the Cartesian coordinate system, where  $\langle S_i \rangle = \langle \psi | \sigma_i | \psi \rangle / 2$ . Here  $|\psi\rangle$  is the free electron wave function (spinor) and  $\sigma_i$  are the Cartesian projections of the Pauli matrices. As mentioned, the spin surface of the free electron is a sphere [5]. The spherical symmetry reflects the fact that all directions of the spin in the vacuum are equally probable. The spin surface of a free hole in the valence band is defined in a similar manner:

$$\langle \mathbf{S} \rangle_n = \langle f_n(\mathbf{k}) | \mathbf{S} | f_n(\mathbf{k}) \rangle, \quad (19)$$

where Cartesian components of  $\mathbf{S}$  are given by Eq. (8) and  $|f_n(\mathbf{k})\rangle$  is the  $n$ th band hole-spinor in the representation (1). Normally the spinor  $|f_n(\mathbf{k})\rangle$  is expressed through the band parameters of the semiconductor and, therefore, has very complicated form in the initial basis used in constructing the wurtzite and zinc-blende Hamiltonians [16, 17]. However, in the energy representation, as we shall see,  $|f_n(\mathbf{k})\rangle$  may be very simple if it is expressed in a parametrized form. In the latter case  $|f_n(\mathbf{k})\rangle$  describes all possible spin states

of the hole having a given wave vector  $\mathbf{k}$  and band index  $n$ , i. e., when the hole is propagating ballistically as a plane wave in the  $n$ th energy band. The parametrized spinor in the energy representation can be related to  $Y$  representation, if the unitary transformation matrix  $T$  between the two representations is known:

$$|f_n(\mathbf{k})\rangle = T|\psi_n(\mathbf{k})\rangle. \quad (20)$$

In the examples considered below, where the ballistic hole has a wave vector perpendicular or parallel to  $c$  axis, the corresponding transformation matrices are given by Eqs. (12) and (16).

#### 4.1. $\mathbf{k} \perp c$ case

The CH band spinor in the energy representation that agrees with the band order in the diagonalized Hamiltonian (11) has the following parametrized form:

$$|\psi\rangle_{c\perp} = (\cos \theta, 0, 0, \sin \theta e^{i\varphi}, 0, 0), \quad (21)$$

where the parameters  $\theta$  and  $\varphi$  define all possible hole spin states in the CH band. By allowing different values for  $\theta$  and  $\varphi$ , as we shall see, one changes the spin magnitude and direction. After the transformation of  $|\psi\rangle_{c\perp}$  to  $Y$  representation,  $|f\rangle_{c\perp} = T_{\perp}^{\dagger}|\psi\rangle_{c\perp}$ , the average spin (19) is found to be

$$\begin{aligned} \langle \mathbf{S} \rangle_{c\perp} &= \langle f | \mathbf{S} | f \rangle_{c\perp} \\ &= -\frac{1}{2} \begin{pmatrix} \cos 2\theta \cos \phi - \sin 2\theta \sin \varphi \sin \phi \\ \cos 2\theta \sin \phi + \sin 2\theta \sin \varphi \cos \phi \\ \sin 2\theta \cos \varphi \end{pmatrix}, \end{aligned} \quad (22)$$

where  $\phi = \tan^{-1}(k_y/k_x)$  is the azimuthal angle of the wave vector  $\mathbf{k}_t$ . If one tries to draw a three-dimensional surface parametrically in the spin space one will find that the Cartesian spin components (22) describe the sphere of radius  $1/2$ , the points on which correspond to different values of the parameters  $\theta$  and  $\varphi$ . The square of the vector  $\langle \mathbf{S} \rangle_{c\perp}$  equals  $1/4$  and is independent of the parameters  $\theta$  and  $\varphi$  as well as of the azimuthal angle  $\phi$ . Thus, for the CH band the spin surface is a sphere and all directions of the hole spin are equivalent under the approximations used. However, for the remaining bands, as we shall see, this is not the case.

The parametrized form of the light-mass band spinor is

$$|\psi\rangle_{l\perp} = (0, \cos \theta, 0, 0, \sin \theta e^{i\varphi}, 0). \quad (23)$$

The average Cartesian components of the hole spin now have a more complicated form:

$$\begin{aligned} \langle \mathbf{S} \rangle_{l\perp} &= \langle f | \mathbf{S} | f \rangle_{l\perp} \\ &= \frac{1}{2} \begin{pmatrix} \frac{A_5 k_t^2 (\cos 2\theta \cos \phi + \sin 2\theta \sin \varphi \sin \phi)}{\sqrt{A_5^2 k_t^4 + 4\Delta_2^2}} \\ \frac{A_5 k_t^2 (\cos 2\theta \sin \phi - \sin 2\theta \sin \varphi \cos \phi)}{\sqrt{A_5^2 k_t^4 + 4\Delta_2^2}} \\ \sin 2\theta \cos \varphi \end{pmatrix}. \end{aligned} \quad (24)$$

As the parameters  $\theta$  and  $\varphi$  are varied, the end of the average spin (24) in the spin space draws a spheroid, whose rotation axis is parallel to  $c$  axis. In the limiting case of small wave vectors,  $k_t \rightarrow 0$ , the spin surface reduces to a line perpendicular to  $k_t$  and parallel to  $c$  axis:  $\langle \mathbf{S}(k_t = 0) \rangle_{l\perp} = (0, 0, \sin 2\theta \cos \varphi)/2$ . Thus, at small wave vectors  $k_t$  the light-hole spin will be perpendicular to the hole propagation direction. In the opposite limit, when  $k_t$  is large, the spin surface (24) reduces to a sphere of radius  $1/2$ . At the intermediate  $k_t$  values the spin surface is a spheroid. Equation (24) yields that the distance from the centre to any point on the spheroid is

$$|\langle \mathbf{S} \rangle_{l\perp}| = \frac{1}{2} \sqrt{\frac{A_5^2 k_t^4 + 4\Delta_2^2 \sin^2 2\theta \cos^2 \varphi}{A_5^2 k_t^4 + 4\Delta_2^2}}, \quad (25)$$

from which it follows that the major axis ( $\theta = \pi/4$ ,  $\varphi = 0$ ) of the spheroid is  $1/2$ , while the minor axis ( $\theta = 0$ ) is equal to  $\{1 + [2\Delta_2/(A_5 k_t^2)]^2\}^{-1/2}/2$ . At CH and LH band crossing, where the transverse wave vector is expressed by Eq. (10) and is  $k_t \approx 0.028 \text{ \AA}^{-1}$  for GaN (Fig. 2), one has that  $2\Delta_2/(A_5 k_t^2) \approx 0.355$ . Thus, in the case of GaN the minor axis at the intersection point is  $\approx 0.47$ , i. e. the spin surface is close to a sphere at the band intersection point. Figure 4 shows the contours of spin surfaces calculated with Eq. (24) in the plane  $\langle S \rangle_z - \langle S \rangle_t$ , where  $\langle S \rangle_t = \sqrt{\langle S \rangle_x^2 + \langle S \rangle_y^2}$ , for GaN at various values of  $k_t$ .

The parametrized form of the heavy-mass band wave function is

$$|\psi\rangle_{h\perp} = (0, 0, \cos \theta, 0, 0, \sin \theta e^{i\varphi}). \quad (26)$$

Calculations with the wave function (26) show that the overall shape of the heavy-hole spin surface is similar to that of light-hole. Figure 5 shows the heavy-hole spin surface at a small magnitude of the wave vector (cf. also Fig. 4). It is an ellipsoid of rotation with the major axis of length  $1/2$  that is parallel to  $\langle S \rangle_z$ . Here it

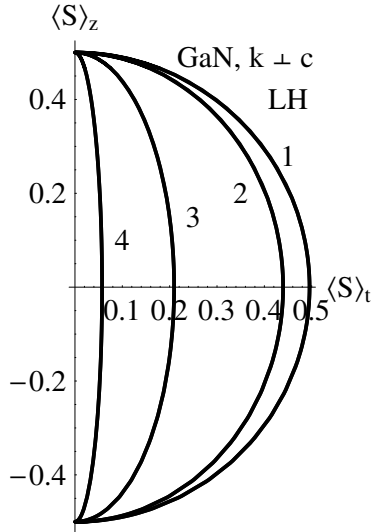


Fig. 4. Contours of spin surfaces of the LH band at various magnitudes of the transverse wave vector  $k_t$  (in  $\text{\AA}^{-1}$ ): (1) 0.0454, (2) 0.0227, (3) 0.0113, and (4) 0.0057. The three-dimensional spin surface can be obtained after rotation of the contours about the vertical axis.

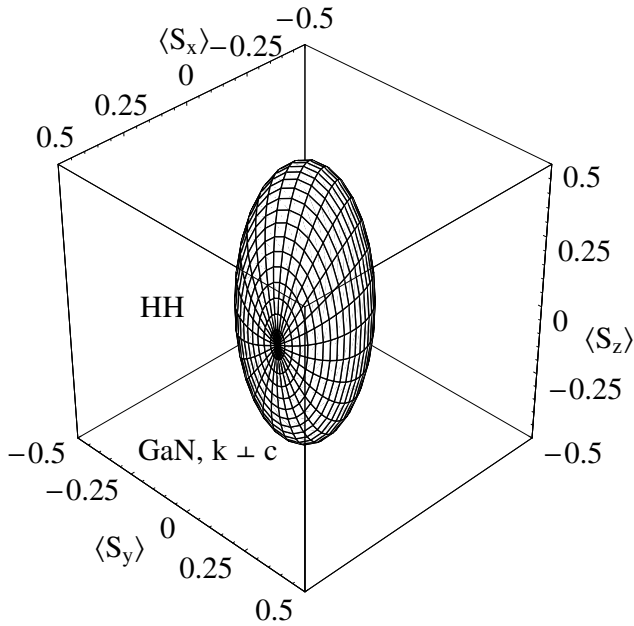


Fig. 5. The spin surface of the heavy-hole band at the transverse wave vector  $k_t = 0.0113 \text{\AA}^{-1}$  and  $\phi = \pi/8$ .

should be pointed out that the shape of the spin surface is invariant with respect to a particular form of the parametrized spinor used to visualize the surface. Different parametrizations will give different geodesic lines that run over the same spin surface and locations of poles where the geodesic lines meet. In Fig. 5 the poles meet on sides of the spheroid rather than on  $\langle S \rangle_z$  axis as one would expect. To have the poles on  $\langle S \rangle_z$

axis a different parametrization should be selected. If the azimuthal direction  $\phi$  of the transverse wave vector  $\mathbf{k}_t$  is changed, the pattern of poles and geodesic lines in Fig. 5 will rotate around  $\langle S \rangle_z$  axis, however, the shape of the spin surface, as should be, will remain an invariant. Therefore, it is safe to set  $\phi = 0$  in the geodesic line formulas (22) and (24).

#### 4.2. $\mathbf{k} \parallel c$ case

As mentioned in Section 3, the transformation formula (16) for a hole moving along the hexagonal axis is exact. The simplest expression for the spin surface in this case is for the heavy-mass band hole. Using the parametrized form of the wave function  $|\psi\rangle_{h\parallel}$ , which coincides with  $|\psi\rangle_{h\perp}$ , one finds that the spin surface, in fact, reduces to a line:

$$\langle \mathbf{S} \rangle_{h\parallel} = \frac{1}{2} \begin{pmatrix} 0 \\ 0 \\ \sin 2\theta \cos \varphi \end{pmatrix}. \quad (27)$$

Thus, the average heavy-hole spin is always parallel to  $k_z$  and lies in the range from  $-1/2$  to  $1/2$ , i.e. in this case independent of  $\theta$  and  $\varphi$  values one has  $\langle \mathbf{S} \rangle_{h\parallel} \parallel k_z \parallel c$ . However, the expressions for spin components of light and crystal-field split-off bands are more complicated.

For the crystal-field split-off band the calculations give the following average spin:

$$\langle \mathbf{S} \rangle_{c\parallel} = \frac{1}{2w(u-w)} \times \begin{pmatrix} 16\Delta_3^2 \cos 2\theta \\ 16\Delta_3^2 \sin 2\theta \sin \varphi \\ \frac{[(u-w)^2 + 32\Delta_3^2][w(u-w) + 32\Delta_3^2]}{2w(-u+w)} \\ \times \sin 2\theta \cos \varphi \end{pmatrix}, \quad (28)$$

where  $u$  and  $w$  is defined by Eq. (14) and (15), respectively. In the limit  $k_z \rightarrow 0$  the components of Eq. (28) reduce to

$$\langle \mathbf{S}(k_z = 0) \rangle_{c\parallel} = - \begin{pmatrix} \frac{2\Delta_3^2 \cos 2\theta}{\delta(-\Delta_1 + \Delta_2 + \delta)} \\ \frac{2\Delta_3^2 \sin 2\theta \sin \varphi}{\delta(-\Delta_1 + \Delta_2 + \delta)} \\ \frac{(\Delta_1 - \Delta_2) \sin 2\theta \cos \varphi}{2\delta} \end{pmatrix}, \quad (29)$$

where  $\delta = \sqrt{(\Delta_1 - \Delta_2)^2 + 8\Delta_3^2}$ . For parameters of GaN Eq. (29) gives

$$\langle \mathbf{S}(k_z = 0) \rangle_{c\parallel} = - \begin{pmatrix} 0.466 \cos 2\theta \\ 0.466 \sin 2\theta \sin \varphi \\ 0.432 \sin 2\theta \cos \varphi \end{pmatrix}.$$

Thus, for small wave vectors the spin surface appears to be close to a sphere. However, in the opposite limit, when  $k_z \rightarrow \infty$ , the spin components describe a line-shaped surface:

$$\langle \mathbf{S}(k_z = \infty) \rangle_{c\parallel} = -\frac{1}{2} \begin{pmatrix} 0 \\ 0 \\ \sin 2\theta \cos \varphi \end{pmatrix}.$$

The parametrized wave function of the light hole  $|\psi\rangle_{l\parallel} = (0, \cos \theta, 0, 0, \sin \theta e^{i\varphi}, 0)$  gives the following average spin:

$$\langle \mathbf{S} \rangle_{l\parallel} = \frac{1}{2[u(u+w) + 32\Delta_3^2]} \times \begin{pmatrix} -16\Delta_3^2 \cos 2\theta \\ -16\Delta_3^2 \sin 2\theta \sin \varphi \\ u(u+w) \sin 2\theta \cos \varphi \end{pmatrix}. \quad (30)$$

In Eq. (30) it was assumed that  $\phi = 0$ . For small wave vectors,  $k_z \rightarrow 0$ , the expression (30) goes to

$$\langle \mathbf{S}(k_z = 0) \rangle_{l\parallel} = \begin{pmatrix} -\frac{2\Delta_3^2 \cos 2\theta}{8\Delta_3^2 + (\Delta_1 - \Delta_2)(\Delta_1 - \Delta_2 + \delta)} \\ -\frac{2\Delta_3^2 \sin 2\theta \sin \varphi}{8\Delta_3^2 + (\Delta_1 - \Delta_2)(\Delta_1 - \Delta_2 + \delta)} \\ \frac{(\Delta_1 - \Delta_2) \sin 2\theta \cos \varphi}{2\delta} \end{pmatrix}. \quad (31)$$

For GaN parameters this equation gives a cigar-shaped spin surface:

$$\langle \mathbf{S}(k_z = 0) \rangle_{l\parallel} = \begin{pmatrix} -0.034 \cos 2\theta \\ -0.034 \sin 2\theta \sin \varphi \\ 0.432 \sin 2\theta \cos \varphi \end{pmatrix}.$$

At a large wave vector,  $k_z \rightarrow \infty$ , Eq. (30) reduces to the formula for a line-shaped spin surface:

$$\langle \mathbf{S}(k_z = \infty) \rangle_{l\parallel} = \frac{1}{2} \begin{pmatrix} 0 \\ 0 \\ \sin 2\theta \cos \varphi \end{pmatrix}. \quad (32)$$

Thus, in the case of the light hole, the spin surface is strongly elongated along  $c$  axis for all wave vector magnitudes. This is similar to HH band holes, for which the spin surface is strictly line-shaped for all wave vector  $k_z$  values.

## 5. Discussion and conclusions

From the presented formulas for the hole spin vector  $\langle \mathbf{S} \rangle$  it is evident that in two important cases, when  $\mathbf{k} \perp c$  and  $\mathbf{k} \parallel c$ , the spin surfaces are ellipsoids of revolution (spheroids), with the length of the minor axis depending on the wave vector magnitude and the valence band parameters. Numerical calculations are needed to prove that this conclusion remains true in a more general case, when the wave vector  $\mathbf{k}$  is pointing in an arbitrary direction. In the case when  $\mathbf{k} \parallel c$ , the obtained expressions are exact.

In both cases, when the hole wave vector is parallel and perpendicular to  $c$  axis, the spin surfaces of the crystal-field split-off band were found to be spherical or close to spherical. This means that for CH holes all spin directions are possible when the hole is moving along or perpendicular to the hexagonal axis.

For heavy-mass and light-mass holes the spin surfaces were found to be spheroids of revolution with the rotation axis parallel to  $c$  axis. Depending on the magnitude of the hole wave vector the spheroid may reduce to a sphere or line. Usually for small wave vectors the surfaces are cigar-shaped and aligned along  $c$  axis. For large wave vectors they are spherical. However, there is an exception from this rule: the spin of the heavy-mass hole propagating along  $c$  axis, as follows from the exact results, is line-shaped for all magnitudes of  $k_z$ .

In [7] the fourteen-fold anisotropy of electrical spin injection efficiency between spin directions perpendicular and parallel to the hole current flow was observed in ferromagnet-semiconductor heterostructures  $\text{Ga}_{1-x}\text{Mn}_x\text{As}/\text{GaAs}$  with  $x = 0.045$  or  $0.035$ . The experimentally detected anisotropy was explained in [6, 9] by line-shaped spin surfaces characteristic of heavy holes in  $\text{A}_3\text{B}_5$  compounds. When the injected spin is parallel to the heavy-hole wave vector the in-

jected hole could propagate ballistically in the undoped GaAs. However, when the spin of the injected hole is perpendicular to the heavy-hole wave vector the injection is inefficient, since such heavy-hole states are forbidden in GaAs and, as we have seen, they may also be forbidden in GaN. By the same reasoning the spin injection anisotropy into GaN is expected too, because, as shown in this paper, the spin surfaces in this material in general case are not spheres. However, the anisotropy is expected to be somewhat smaller due to smaller differences between the valence-band effective masses (or equivalently, density of states) in GaN as compared to GaAs.

In conclusion, the paper shows that the hole spin surfaces in the wurtzite-type semiconductors are ellipsoids of rotation, which at small and large wave vectors may reduce to a sphere or line. As a result, the anisotropy of the spin injection efficiency in these materials is predicted, too.

## References

- [1] I. Žutić, Spintronics: Fundamentals and applications, *Rev. Mod. Phys.* **76**(2), 323–410 (2004).
- [2] S.J. Pearton, C.R. Abernathy, M.E. Overberg, G.T. Thaler, D.P. Norton, N. Theodoropoulos, A.F. Hebard, Y.D. Park, F. Ren, J. Kim, and L.A. Boatner, Wide band gap ferromagnetic semiconductors and oxides, *J. Appl. Phys.* **93**(1), 1–13 (2003).
- [3] W. Prellier, A. Fouchet, and B. Mercey, Oxide-diluted magnetic semiconductors: A review of the experimental status, *J. Phys.: Condens. Matter* **15**(37), R1583–R1601 (2003).
- [4] A. Dargys, Coherent properties of hole spin, *Lithuanian J. Phys.* **43**(2), 123–128 (2003).
- [5] A. Dargys, Spin surfaces and trajectories in valence bands of tetrahedral semiconductors, *Phys. Status Solidi B* **241**(1), 145–154 (2004).
- [6] A. Dargys, Hole spin surfaces in  $A_3B_5$  compounds, *Phys. Status Solidi B* **241**(13), 2954–2961 (2004).
- [7] D.K. Young, E. Johnston-Halperin, D.D. Awschalom, Y. Ohno, and H. Ohno, Anisotropic electrical spin injection in ferromagnetic semiconductor heterostructures, *Appl. Phys. Lett.* **80**(9), 1598–1600 (2002).
- [8] A. Dargys, Ultrafast control of hole spin by electric field in semiconductors, *IEEE J. Selected Topics Quantum Electron.* **10**(1), 155–158 (2004).
- [9] A. Dargys, Hole dynamics under  $\pi$ -pulse excitation, *Phys. Rev. B* **70**(12), 125207-1–11 (2004).
- [10] A. Dargys, Control of valence-band hole spin by electric field, *Acta Phys. Pol. A* **105**(3), 295–306 (2004).
- [11] G.L. Bir and G.E. Pikus, *Symmetry and Strain-Induced Effects in Semiconductors* (Wiley, New York, 1974) Chap. 5.
- [12] E.O. Kane, The  $\mathbf{k} \cdot \mathbf{p}$  method, in: *Semiconductors and Semimetals*, Vol. 1, eds. R.K. Willardson and A.C. Beer (Academic Press, New York, 1966) p. 75–99.
- [13] S.L. Chuang and C.S. Chang,  $\mathbf{k} \cdot \mathbf{p}$  method for strained wurtzite semiconductors, *Phys. Rev. B* **54**(4), 2491–2504 (1996).
- [14] G.B. Ren, Y.M. Liu, and P. Blood, Valence-band structure of wurtzite GaN including the spin–orbit interaction, *Appl. Phys. Lett.* **74**(8), 1117–1119 (1999).
- [15] D. Fritsch, H. Schmidt, and M. Grundmann, Bandstructure pseudopotential calculation of zinc-blende and wurtzite AlN, GaN, and InN, *Phys. Rev. B* **67**(23), 235205-1–13 (2003).
- [16] M. Tiersten, Acoustic-mode scattering of holes, *IBM J. Res. Develop.* **5**(April), 122–131 (1961).
- [17] F. Szmulowicz and F.L. Madarasz, Angular dependence of hole–acoustic-phonon transitions rates in silicon, *Phys. Rev. B* **26**(4), 2101–2112 (1982).

## SKYLĖS SUKINIO PAVIRŠIAI VIURCITO GARDELĖS PUSLAIDININKIUOSE

A. Dargys

*Puslaidininkų fizikos institutas, Vilnius, Lietuva*

### Santrauka

Išnagrinėtos laisvosios skylės, kuri juda arba sunkiosios, arba lengvosios masės energetinėje juostoje, arba atskilusioje dėl kristalinio elektrinio lauko juostoje, sukinių savybės nuo valentinės juostos parametrų ir skylės bangos vektoriaus krypties bei dydžio. Rasti analiziniai sprendiniai, kurie aprašo vidutinį sukinių dviem svarbiais atvejais: kai balistinės skylės bangos vektorius nukreiptas

arba lygiagrečiai, arba statmenai kristalo heksagonalinei ašiai. Parodyta, kad abiem atvejais sukinių paviršiai yra sferoidai. Priklausomai nuo skylės bangos vektoriaus ilgio bei krypties, o taip pat nuo valentinės juostos parametrų, sukinių paviršiai gali transformotis į sferą arba į tiesę. Skylės sukinių paviršių savybės pailiustruotos GaN – puslaidininkio, kuriame vyrauja kristalinis laukas – atveju.